

ARTICLE

Open Access

Tumor microenvironment-responsive metal nanotherapeutics for breast cancer chemo-/immunotherapy

Jinggong Liu^{1,2}, Wenyong Li¹, Yongpeng Lin², Yongjun Peng¹, Meixiao Zhan¹, Haoqiang Lai³, Yanzhou Chang³, Yongjin Li², Ka-hing Wong⁴, Bolai Chen^{1,2} and Tianfeng Chen^{1,3}

Abstract

Many metal complexes not only had excellent cytotoxic antitumor effects but also could function as a positive immunomodulatory to improve antitumor effects by modifying the local tumor microenvironment. Herein, a dual-target nanotherapeutics (MP3/ACPP/AE105@NPs) with uPAR targeting and tumor microenvironment-responsive ability was developed by using AE105 as the targeting ligand and ACPP as the tumor microenvironment-responsive peptide to locate the metal complex to cells. Assisted by the surface modification, MP3/ACPP/AE105@NPs demonstrated excellent cellular uptake of the drugs in in vitro experiments, thereby enhancing the therapeutic utility of the loaded metal complex. The nanotherapeutics induced the excessive ROS generation by inhibiting the activity of TrxR and modulated those proteins which were related to metastasis through inhibiting ERK/AKT activation mediated by FAK in MDA-MB-231 cells. This nanotherapeutics could also significantly improve the therapeutic benefits in vivo accompanied by reduced toxic side effects. Importantly, MP3/ACPP/AE105@NPs treatment stimulated immunotherapeutic response, which was indicated by the activation of tumor-infiltrated cytotoxic T cells, and improved the maturation of dendritic cells (DCs), and the proliferation-inhibitory effect of tumor-associated M2 macrophages. Taken together, the results suggested that this dual-targeted nanotherapeutics offered new opportunities for boosting the synergistic treatment of breast cancer with chemotherapy and immunotherapy.

Introduction

Despite rapid advances in diagnostic and therapeutic procedures, the alarming incidence rate of cancer reminds us that it remains one of the most devastating diseases in the world to date, affecting millions of people worldwide^{1–8}. Nowadays, cisplatin and other platinum (Pt)-based drugs have been widely used in clinical treatment of cancer

accompanied by toxic effects on normal organs⁹. Significant efforts have been devoted to developing other metal complexes as Pt-based drugs alternatives because of their positive therapeutic efficiency as a tumor eliminative. A ruthenium polypyridyl complex named RuPOP, which was found to have potent antitumor activity against MDA-MB-231 cells by inhibiting the proliferation and metastasis¹⁰. A gold (III) porphyrin complex named MP3 was able to activate the mitochondria dysfunctions to promote intrinsic cell apoptosis involvement in TrxR inhibition¹¹. Many exciting outcomes in the field of oncology immunology confirmed that chemotherapy could initiate an immune response and function as a positive immunomodulatory to improve antitumor effects by modifying the local tumor microenvironment through multiple mechanisms. Some chemotherapeutic drugs could stimulate the generation of

Correspondence: Yongjun Peng (sxpj2196@163.com) or Bolai Chen (chenbolai@gzucm.edu.cn) or Tianfeng Chen (tchentf@jnu.edu.cn)

¹Guangdong Provincial Key Laboratory of Tumor Interventional Diagnosis and Treatment, Zhuhai Interventional Medical Center, Zhuhai People's Hospital (Zhuhai Hospital Affiliated with Jinan University), Jinan University, 519000 Zhuhai, P.R. China

²Orthopedics Department, Guangdong Provincial Hospital of Traditional Chinese Medicine, The Second Affiliated Hospital of Guangzhou University of Chinese Medicine, No. 111 Dade Road, 510120 Guangzhou, China

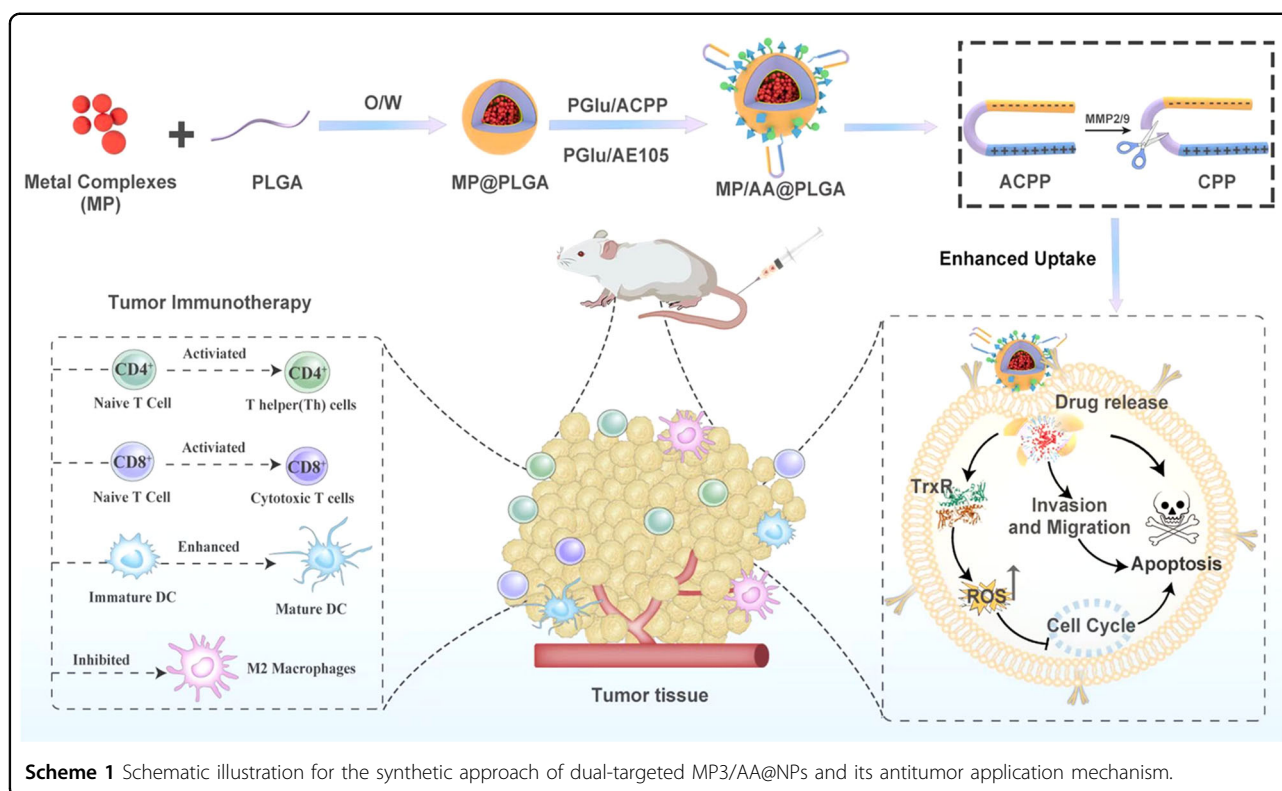
Full list of author information is available at the end of the article

These authors contributed equally: Jinggong Liu, Wenyong Li, Yongpeng Lin

© The Author(s) 2023



Open Access This article is licensed under a Creative Commons Attribution 4.0 International License, which permits use, sharing, adaptation, distribution and reproduction in any medium or format, as long as you give appropriate credit to the original author(s) and the source, provide a link to the Creative Commons license, and indicate if changes were made. The images or other third party material in this article are included in the article's Creative Commons license, unless indicated otherwise in a credit line to the material. If material is not included in the article's Creative Commons license and your intended use is not permitted by statutory regulation or exceeds the permitted use, you will need to obtain permission directly from the copyright holder. To view a copy of this license, visit <http://creativecommons.org/licenses/by/4.0/>.



immunomodulatory responses by activating tumor-specific cytotoxic T lymphocytes, promoting the maturation of DC cells and the rearrangements of the phenotypic subtypes of tumor-associated macrophages (TAMs), which contributed to their sustained therapeutic effects^{1,12}. Studies reported that cisplatin could boost the T-cell activity in AT-3 tumor-bearing mice¹³. We have found in our previous study that RuPOP could potentiate immune responses of NK cells via reprogramming immuno-microenvironment in MDA-MB-231 cells¹⁴. Therefore, developing chemotherapeutic agents to integrate chemotherapy and potential immunotherapy are encouraging approaches for the cancer treatment. Nevertheless, the potential role of MP3 in tumor immunotherapy is unclear. In addition, accumulating evidence showed that the broader targeted chemotherapy implementation of metal chemotherapeutic complexes in clinical practice were severely hindered by the off-target toxicity and poor specificity under physiological conditions¹⁵.

Encouragingly, poly (lactide-co-glycolide) (PLGA) has been well proven to be an excellent delivery system for cancer therapy on account of its outstanding biocompatibility and biodegradability¹⁶. However, the delivery system of free PLGA showed hydrophobicity and was not able to distinguish between the normal and cancer cells. Therefore, it is significant to functionalize with the hydrophilic polymer and specific recognition ligands on the surface of the nanoparticles to achieve therapeutic efficiency and specificity¹⁷. Bearing all the above factors in mind, three

dual-targeted nanotherapeutics were fabricated by coating metal complexes loaded PLGA nanocores with ACPP and AE105 peptides. In this study, MP3/ACPP/AE105@NPs (MP3/AA@NPs) was used to integrate chemotherapy and immunotherapy for treating breast cancer. ACPP peptide is sensitive to the matrix metalloproteinases-2 (MMP-2), which could be recognized and cleaved by MMP-2 over-expressed at the tumor tissue, facilitating the entry of nanoparticles into tumor cells without significant cytotoxicity¹⁸. AE105 peptide exhibits extremely high potency as a targeting ligand for the urokinase plasminogen activator receptor (uPAR) and the metastasis and invasion of MDA-MB-231 cells are closely associated with uPAR¹⁹. The synthesized MP3/AA@NPs amplified its inhibitory effects on TrxR and modulated the expression of metastasis-related proteins through inhibiting ERK/AKT activation mediated by FAK in MDA-MB-231 cells. Furthermore, the administration of MP3/AA@NPs could significantly improve the therapeutic benefits in MDA-MB-231-, and 4T1-bearing mouse models accompanied by the activation of immunotherapeutic response (Scheme 1).

Materials and methods

Materials

PLGA (LA: GA = 75:25, MW 50000), TPGS (D- α -tocopherol acid polyethylene glycol 1000 succinate), PGlu (polyglutamic acid), PEI (Polyetherimide), NHS (N-Hydroxy succinimide), EDC (1-(3-Dimethylaminopropyl)-

3-ethylcarbodiimide hydrochloride), Cisplatin, MTT (thiazolyl blue tetrazolium bromide), NADPH (Nicotinamide Adenine Dinucleotide Phosphate) and DNTB (5,5'-Dithiobis (2-nitrobenzoic acid) were obtained from Sigma-Aldrich. ACPP peptide (sequence E8-PLGLAG-R9-C) and AE105 (uPAR-binding peptide) were purchased from GL Biochem (Shanghai) Ltd. Hoechst 33258, Lysotracker (red), BCA kits, acetonitrile and N,N-dimethylformamide (DMF) were purchased from Thermo Fisher Scientific (China) Co., Ltd. Dulbecco's modified Eagle's medium (DMEM) and fetal bovine serum (FBS) were purchased from Gibco (Rockville, MD, USA). Three metal complexes (MP) used in this study, including cisplatin, ruthenium polypyridyl complex RuPOP, and gold (III) porphyrin complex, were referred as MP1, MP2, and MP3, respectively. RuPOP and gold (III) porphyrin complex were prepared as our former methods^{20,21}.

Synthesis of PGlu/ACPP and PGlu/AE105

A mixture of 25 mg ACPP (2.45 μ mol) and 1 mL PGlu (0.5 mg/mL) was added into a solution of EDC (250 μ L, 0.1 mol/L) and NHS (250 μ L, 0.1 mol/L) dissolved in 1 mL PEI (20 mg/mL). PGlu/ACPP was obtained after stirring the above solution at room temperature for 24 h and dialyzing (MWCO = 6000) against distilled water for another 24 h. The PGlu/AE105 was prepared by the same method except using AE105 (10 mg, 2.45 μ mol) instead of ACPP (25 mg, 2.45 μ mol).

Preparation of MP@PLGA

A general method for the preparation of MP1@PLGA, MP2@PLGA, MP3@PLGA were as follow. Briefly, an organic phase consisting of PLGA (5 mg/mL) and metal complexes (MP, 2 mg/mL) dissolved in 2 mL acetonitrile was added dropwise into a solution of 6 mg TPGS (1 mg/mL). Following equilibration of the mixture at 4 °C for 30 min, MP@PLGA was purified by dialysis for further use.

Fabrication of surface-modified MP/AA@NPs

A general method for the preparation of MP1/AA@NPs, MP2/AA@NPs, MP3/AA@NPs were as follow. In the first step, MP@PLGA-NHS ester was generated by activating the terminal carboxylic acid group of MP@PLGA with EDC/NHS in DMF solution. In the following step, PGlu/ACPP or PGlu/AE105 (molar ratio 1.5:1) was then added into the above solution and stirred continuously for 24 h with the protection of N₂, resulting in the MP/ACPP@NPs and MP/AE105@NPs, respectively. While both the PGlu/ACPP and PGlu/AE105 were added into a solution of DMF dissolved with the activated MP@PLGA to prepared the dual-targeted MP3/AA@NPs. The fluorescent coumarin-6/ACPP@NPs, coumarin-6/AE105@NPs and coumarin-6/AA@NPs were prepared by using the same method.

Characterization of MP3/AA@NPs

AFM, TEM, and UV-vis spectrophotometry were used to characterize the structure and morphology of MP3/ACPP@NPs, MP3/AE105@NPs and MP3/AA@NPs. The size and zeta potential of the nanoparticles were determined by using Zetasizer nano ZS analyzer.

Cell lines and in vitro cytotoxicity

All the cells used in this study, including MDA-MB-231 cell line, MCF-7 cell line, 4T1 cell line, HepG2 cell line, R-HepG2 cell line, EJ cell line and L02 cell line were obtained from the American Type Culture Collection (ATCC, Manassas, VA) and were incubated in DMEM supplemented with 10% FBS and 1% penicillin/streptomycin at 37 °C and 5% CO₂ in a humidified incubator. The toxicities of MP3, MP3/ACPP@NPs, MP3@NPs/AE105 and MP3/AA@NPs against these cells were carried out by the MTT after continuous incubation for 72 h.

In vitro cellular uptake of coumarin-6/AA@NPs

The in vitro cellular uptake of coumarin-6/AA@NPs was described as our previous method²². MDA-MB-231 cells or L02 cells were treated with 0.5 mg/mL of coumarin-6/ACPP@NPs, coumarin-6/AE105@NPs and coumarin-6/AA@NPs with the density 40×10^4 cells/well (2 mL) in six-well plates for the indicated time. After incubation, the uptake amounts of various nanoparticles were quantified according to the fluorescence intensity of coumarin-6 by utilizing a fluorescence microplate reader (Spectra Max M5, Bio-Tek). The same method was used to measure the uptake of nanoparticles under different conditions, including fresh DMEM, DMEM, and the tumor stroma cell.

Intracellular colocalization of MP3/AA@NPs

MDA-MB-231 or L02 cells in a 2-cm dishes were incubated with MP3/AA@NPs (labeled with coumarin-6) for 1, 2, 4, and 8 h. The fluorescence images were taken after the cells were stained with Lysotracker Red (DND-99, 80 nM) and DAPI H33258 (1 μ g/mL) for 2 h and 30 min, respectively.

uPAR competing assay

A competitive inhibition assay was performed to study uPAR receptor-mediated uptake of coumarin-6-loaded nanoparticles²³. 8000 cells/well of MDA-MB-231 cells were firstly pre-incubated with different concentrations of AE105 (0.25, 0.5, 1, and 2 mg/mL) for 2 h in 96-well plates before 2 μ M of coumarin-6/AA@NPs were added. The fluorescence intensities of internalized coumarin-6/AA@NPs were measured after incubation for another 4 h.

In vitro drug release of MP3/AA@NPs

The release profile of MP3 from MP3/AA@NPs were measured. In brief, MP3/AA@NPs were dispersed in a cell

lysate or PBS with pH values 7.4 or 5.3. After that, the acquired solutions were shaking for the predetermined time points and centrifuged (12,000×g) for 30 min. The MP3 in the supernatant was determined by measuring its absorbance at 525 nm.

Wound-healing assay

MDA-MB-231 cells (40×10^4 cells/well) were firstly cultured to six-well plates for 24 h. The resulting confluent cell monolayers were then wounded with pipette tips after starvation for 4 h by the addition of (3% FBS) DMEM. The cells were incubated with different concentrations of MP3/AA@NPs or MP3 for 24 h in the fresh DMEM supplement with 3% FBS after rinsing with PBS. After incubation, cells were photographed again at three random areas after the addition of 2 μ L Hoechst for 30 min.

Transwell invasion assay

Transwell experiments was applied to investigate the effect of MP3/AA@NPs and MP3 on MDA-MB-231 cell invasion in Transwell Boyden chamber (8-mm pore, Corning, Lowell, MA). After 24 h incubation with the indicated concentrations of MP3/AA@NPs (4 nM and 8 nM) and MP3 (8 nM), the invaded cells on the lower face were imaged on a phase-contrast microscope (2003, Nikon TS100) after being fixed and stained.

Flow cytometric analysis of cell cycle distribution

The effects of MP3/AA@NPs and MP3 on the cell cycle distribution were assayed based on flow cytometric analysis. In brief, MDA-MB-231 cells were firstly treated with 0.01 μ M, 0.02 μ M and 0.04 μ M of MP3/AA@NPs or MP3 for 72 h, respectively. Then, 70% ethanol and PI (propidium iodide) were used to fix and stained for 30 min. Finally, the resulting cells were applied to the Epics XL-MCL flow cytometer (Beckman Coulter, Miami, FL) to obtain the cell cycle distribution.

Assessment of intracellular reactive oxygen species (ROS) generation

Dihydroethidium (DHE, Beyotime) was used to determine the generated ROS⁵. MDA-MB-231 cells were incubated with 0.16 μ M and 0.32 μ M MP3/AA@NPs or 0.32 μ M MP3. The ROS levels were recorded on a fluorescence microplate reader from 0 to 120 min, and the cells images were taken at 0, 20, 80, and 120 min.

Determination of TrxR activity

The activity inhibition of TrxR by MP3 or MP3/AA@NPs was detected using a Thioredoxin Reductase Assay Kit (Cayman)²⁴. Firstly, the total cellular proteins were extracted and quantified by a BCA assay. Then a mixture of 60 μ g of cytosolic protein, NADPH and DNTB were incubated

with or without MP3 or MP3/AA@NPs for 1 h in 96-well plates. After incubation, the OD values were recorded at 412 nm by a microplate spectrophotometer.

Western blot analysis

The effects of MP3/AA@NPs on the expression levels of proteins related to different cell signaling pathways were examined by western blot analysis, as described previously⁸.

In vivo antitumor efficiency

A study was carried out on female BALB/c mice (6–8 weeks, 16–20 g) to assess the in vivo therapeutic efficiency of MP3 and MP3/AA@NPs. In order to establish tumor mode, each mouse was subcutaneously injected with 100 μ L serum-free medium containing 1×10^6 MDA-MB-231 cells in the right oxtar. Upon reaching a tumor volume of about 100 mm³, the mice were randomly divided into four groups. i.e., PBS group, MP3 (0.50 mg/kg) group, MP3/AA@NPs (0.25 mg/kg) and MP3/AA@NPs (0.50 mg/kg) group and received treatments every other day. Tumor volumes and mouse body weights were measured every four days and every three days, respectively. Tumor volume = (width² × length)/2. After 21 days therapy, the harvested major organs and tumors were weighed and fixed with 4% paraformaldehyde for subjecting to the H&E analysis. The hematological indexes including ALT, CHOL, CREA, HDL-C, LDL-C, and UA of different treatments groups were obtained in the Blood Test Center of Guangzhou Overseas Chinese Hospital. In addition, a clinical magnetic resonance imaging scanner (GE 1.5 T, USA) was applied to study the Standard ADC, Slow ADC signal and Fast ADC signal of different groups at the tumor sites when the mice were sacrificed according to our previous methods²⁵.

Immunogenicity of MP3/AA@NPs In vivo

Using BALB/c nude female mice bearing 4T1 tumors (6–8 weeks, 16–20 g), MP3 and MP3/AA@NPs were evaluated in vivo for their immunomodulatory abilities. The grouping form and the administration method were the same as in the above experiments. The immune-related cell types were screened by flow cytometry analysis when the tumor and spleen were taken out and photographed after 14 days of therapy. CD3-APC (BioLegend, #100236), CD4-APC/Cyanine7 (BioLegend, #100414), and CD8-PE (BioLegend, #100708) antibodies were used to distinguish the cytotoxic T lymphocytes (CD3⁺CD8⁺) and helper T cells (CD3⁺CD4⁺) in T lymphocyte. F4/80-PE (BioLegend, #157304) and CD206-APC (BioLegend, #162506) antibodies were used as the markers of M2 macrophages and dendritic cells (DCs) in the spleen site were stained by antibodies of CD80-PE (BioLegend, #104708) and CD86-APC/Cyanine7 (BioLegend, #105030).

Results and discussion

Rational design and physicochemical characterization of MP3/AA@NPs

In this study, three dual-target nanotherapeutics, including MP1/ACPP/AE105@NPs (MP1/AA@NPs), MP2/ACPP/AE105@NPs (MP2/AA@NPs), and MP3/ACPP/AE105@NPs (MP3/AA@NPs) were successfully fabricated based on nanoprecipitation method and characterized. The synthetic diagram is outlined in Fig. 1A. The synthesized routine and characterization of MP3 were shown in Supplementary Fig. S1. MP3 was first encapsulated into PLGA by the solvent evaporation method, and then the targeting peptides ACPP and AE105 were decorated on the surface of PLGA. The average hydrated size of free PLGA was about 180 nm, and the zeta potential was about -5 mV. A slight increase in the size and a significant reversal of the zeta potential were found after loading with MP3 and modification with the targeting peptide, which changed to 250 nm and $+10$ mV, respectively (Fig. 1D, E). The results of high-resolution TEM and AFM images showed that MP3/AA@NPs was highly dispersed with a smooth surface and diameters of approximately 200 nm (Fig. 1B, C), which was in accordance with the hydrated particle size. Also, these observations proved the successful conjugation of the targeting peptide. In addition, the TEM of MP1/AA@NPs and MP2/AA@NPs were shown in Supplementary Fig. S2. All the above results indicated the universalities of this method for the encapsulation of metal complexes. A similar UV/Vis absorption spectrum could be observed by comparing MP3/AA@NPs with MP3, indicating that MP3 had been successfully loaded into the PLGA (Fig. 1G). The grafting of ACPP and AE105 on the surface of NPs was further confirmed by using a bicinchoninic protein assay. As shown in Fig. 1H, the UV/Vis spectrum showed an increase in absorbance at 562 nm after incubation with the BCA kit for 30 min due to the presence of peptides on the nanoparticles. Finally, MP3/ACPP@NPs, MP3/AE105@NPs, and MP3/AA@NPs in aqueous solution and DMEM (10% FBS) remained stable for 3 days (Fig. 1F and Supplementary Fig. S3).

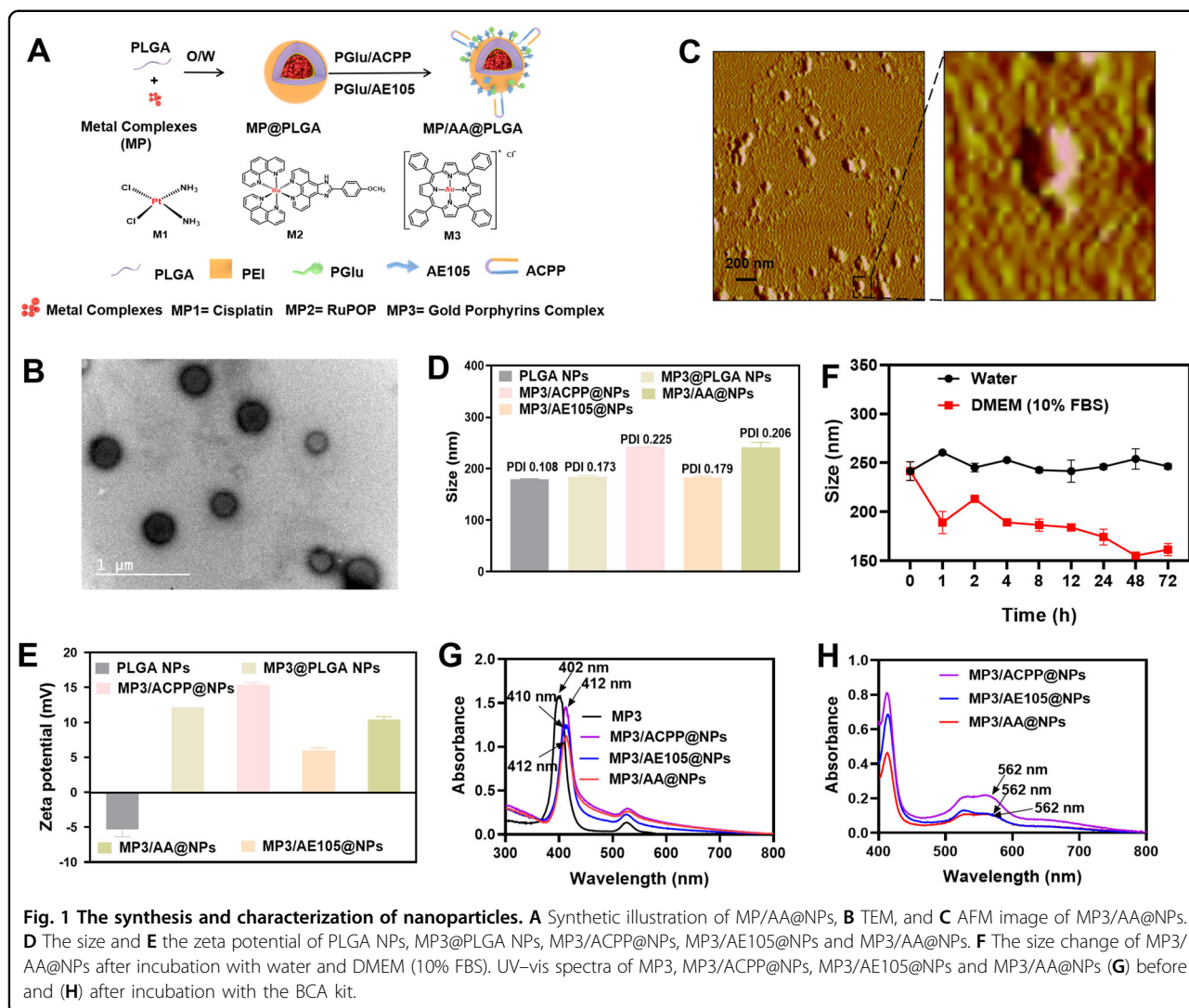
Intracellular localization and bioresponsive drug-release profiles of MP3/AA@NPs

Coumarin-6/AA@NPs was prepared to understand the internalization of MP3/AA@NPs. Real-time monitoring of coumarin-6/AA@NPs absorption and transport (green) was performed in MDA-MB-231 cells, and the lysosomes were labeled with LysoTracker (red). As illustrated in Fig. 2A, a weak green fluorescent signal could be observed in lysosomes after 1 h of cell incubation with coumarin-6/AA@NPs. The green color could be observed throughout the entire cytoplasm after incubation for 2–8 h, suggesting that coumarin-6/AA@NPs could be internalized quickly and was mainly

concentrated in the lysosomes after entering the cell, which was beneficial for tumor therapy. The drug-release behavior is an important parameter of drug-loaded nanoparticles in cancer therapeutics. It had been known that the cargo encapsulated in PLGA nanoparticles was easily released in the tumor microenvironment because the ester bond of PLGA could be degraded under lower pH value and esterase existing in such situations. We also determined the release of MP3 from MP3/AA@NPs after immersion in different mediums for specified time durations. Phosphate-buffered saline (PBS) with a pH of 7.4, pH 5.3, and cell lysates of MDA-MB-231 were used to simulate the body blood, lysosomal internal medium, and in vivo situations, respectively. Figure 2B shows the profiles of the amount of MP3 released from MP3/AA@NPs as a function of time, and Fig. 2C shows the illustration of the degradation diagram of MP3/AA@NPs in lower pH and cell lysate. The results showed a much faster and higher release ratio of MP3 from MP3/AA@NPs in the environment of the MDA-MB-231 lysate compared with the other two environments, but there was no visible drug release could be detected in PBS (pH 7.4), indicating that MP3/AA@NPs was stable during blood circulation. For instance, the accumulated release ratio of MP3 from MP3/AA@NPs was about 8.6% at pH 7.4, 35.8% at pH 5.3, and 49.7% at the MDA-MB-231 cell lysate after 72 h. The corresponding morphological evolution of MP3/AA@NPs was recorded using TEM (Fig. 2D, E). At pH 7.4, the NPs remained intact, which determined the release of MP3, whereas obvious hollow features and degradation of MP3/AA@NPs appeared after 72 h of immersion at pH 5.3, indicating that these NPs could be hydrolyzed in an acid environment. Interestingly, MP3/AA@NPs was almost degraded in MDA-MB-231 cell lysate, which facilitated MP3 release. Overall, these results indicated that when MP3/AA@NPs were absorbed by the cells, the loaded metal complex could be released in the tumor microenvironment, exerting an anticancer effect.

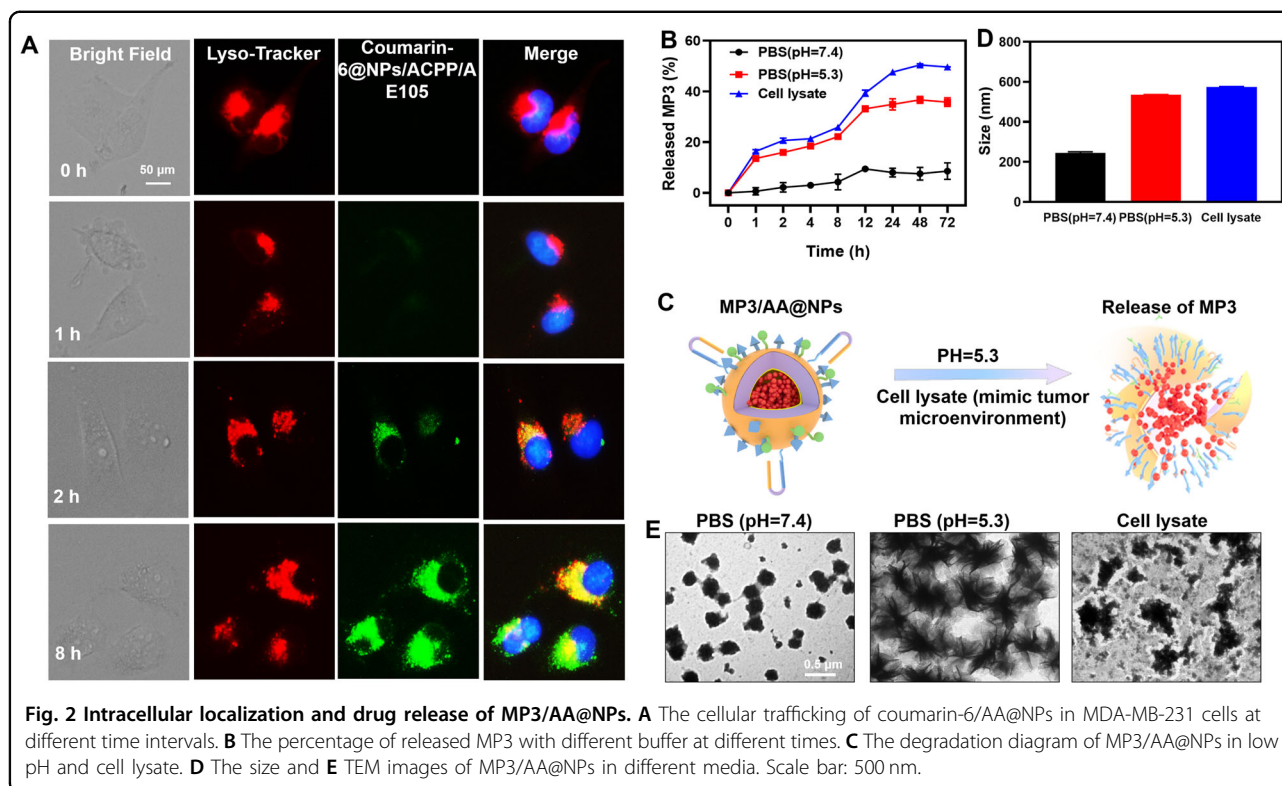
In vitro anticancer activity and cellular uptake of MP3/AA@NPs

This study first investigated the in vitro cytotoxicity of MP3/AA@NPs against a series of cancer cells using the MTT assay by comparing it with the free MP3. The dual-targeted MP3/AA@NPs exhibited a higher proliferation-inhibitory activity against a variety of cancer cells than the free MP3 and the single-targeted NPs, and importantly, MP3/AA@NPs was less toxic to L02 normal human cells (Fig. 3A and Supplementary Table S1). Interestingly, the aggressive MDA-MB-231 cells exhibited the highest sensitivity to MP3/AA@NPs with an IC_{50} value of $0.03 \mu\text{M}$, whereas the IC_{50} value for free MP3 was only $0.15 \mu\text{M}$. The above results might be ascribed to the different absorption of the targeting peptide-containing nanotherapeutics between normal and tumor cells²⁶. The potency of cellular



uptake affects the biological effects of nanoparticles and is a key factor for the success of their clinical applications. AE105 peptide could recognize and bind to uPAR receptor overexpressed on the surface of cancer cells. ACPP peptide could trigger the internalization of nanoparticles after the activation by MMP-2 or matrix metalloprotease (MMP-9) under the tumor microenvironments (Fig. 3B). The cellular uptake behavior of coumarin-6-loaded PLGA nanoparticles was investigated in MDA-MB-231 cells and L02 cells, respectively, for an appointed time (8 h) by testing the fluorescence intensity of coumarin. Compared with coumarin-6/ACPP@NPs and coumarin-6/AE105@NPs, coumarin-6/AA@NPs exhibited a stronger internalizing behavior (Fig. 3D). The cellular uptake of coumarin-6/ACPP@NPs, coumarin-6/AE105@NPs, and coumarin-6/AA@NPs was measured in fresh DMEM, DMEM, and the tumor stroma after 8 h to determine the function of the targeting peptide. The internalizing behavior of coumarin-

6/AA@NPs and coumarin-6/ACPP@NPs was found to be increased the most in the tumor stroma (mimetic tumor microenvironment), followed by in DMEM. However, the cellular uptake of coumarin-6/AE105@NPs had no obvious change in each condition (Fig. 3E). All the above results revealed that the introduction of ACPP peptide stimulated the cellular uptake of nanoparticles via the enhanced interaction of nanoparticles with the cells. Moreover, compared with coumarin-6/ACPP@NPs and coumarin-6/AE105@NPs, an enhanced fluorescence was observed in coumarin-6/AA@NPs-treated cells (Fig. 3C). In addition, the results in Fig. 3F clearly showed that the excess amount of AE105 could dose-dependently block the cellular uptake of MP3/AA@NPs. More importantly, the uptake of MP3/AA@NPs by MDA-MB-231 cells was gradually increased over time, while the accumulation was much less in L02 cells (Fig. 3G). Besides, a positive correlation was found between uPAR expression and enrichment of MP3/



AA@NPs in MDA-MB-231 cells (Fig. 3H). Moreover, the fluorescence images in Fig. 3C were in agreement with the aforementioned results; only a weak fluorescence was observed in L02 cells after 8 h, indicating the poor interaction of coumarin-6/AA@NPs with L02 cells. Collectively, these observations revealed that targeting peptide modification was beneficial for the selective cellular uptake of MP3/AA@NPs into MDA-MB-231 cells.

MP3/AA@NPs suppressed cancer cell migration and invasion and its mechanism

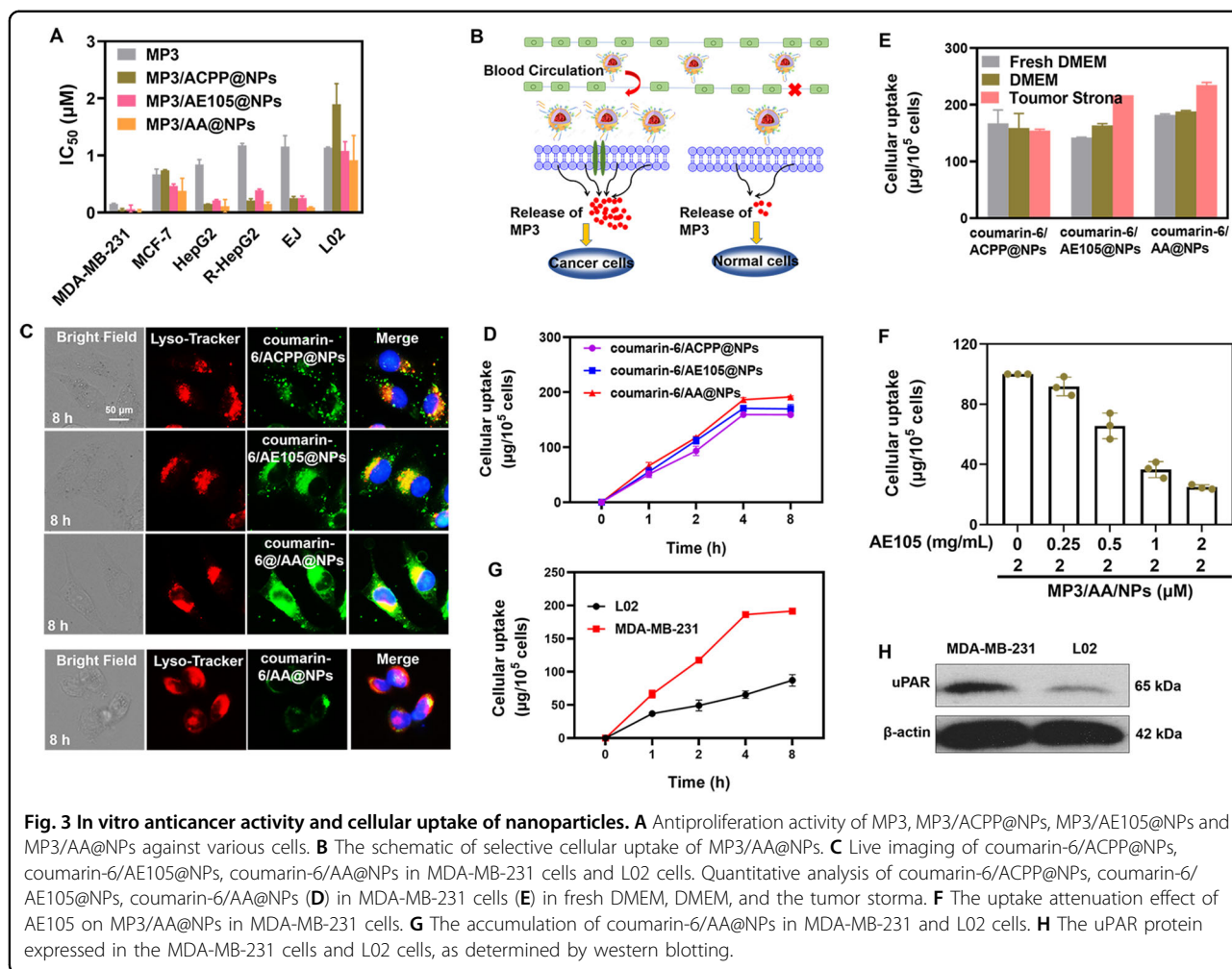
To further clarify the mechanism underlying the exciting cytotoxicity, the impact of MP3/AA@NPs on the invasiveness of MDA-MB-231 cells was subsequently investigated. According to Fig. 4A, MDA-MB-231 cells displayed a notable reduction in migration and invasion following the treatment with MP3/AA@NPs. After 24 h treatment with a slightly toxic concentration (2 nM, 4 nM, and 8 nM; Fig. 4B) of MP3/AA@NPs, the proportion of the migrating and invasive cells were decreased to 74.2%, 55.5%, 35.6%, and 73.6%, 52.1%, 21.3%, respectively. The average migration and the average invasion of the cells were 66.5% and 87.1%, even when the concentration of MP3 was increased to 8 nM (Fig. 4C, D).

It is well known that FAK plays a key regulatory role in tumor proliferation and migration as one kind of cytoplasmic protein tyrosine kinase²⁷. Western blot assays were carried out to detect the total expression level of FAK and its phosphorylated form. Figure 4E shows that phosphorylated

FAK at Tyr397, Tyr925, and Tyr576/577 were significantly decreased after treatment with MP3/AA@NPs, but the total FAK levels were almost unchanged. Recent studies have also revealed that the activation of FAK could stimulate PI3K/AKT and Ras/MEK/ERK signaling pathways, resulting in the overexpression of downstream MMPs and uPA^{27,28}. As shown in Fig. 4F, there were a downregulation of phosphorylated ERK and AKT levels after treatment with MP3/AA@NPs, but no obvious inhibitory effect on the total forms of ERK and AKT. On the other hand, MMPs and uPA are involved in tumor invasion and metastasis. It is possible that breast cancer may promote tumor infiltration by overexpressing MMP-2 and MMP-9. The results in Fig. 4G validated this hypothesis. The expression of MMP-9, MMP-2 and uPA were gradually downregulated as well as the upregulation of TIMP-1 with the increased concentration of MP3/AA@NPs. These results strongly suggested that the antimigration and anti-invasion activities of MP3/AA@NPs against MDA-MB-231 cells could be related to the inactivation of FAK by uPA and MMPs.

MP3/AA@NPs inhibited TrxR activity and stimulated ROS generation

TrxR plays an essential role in regulating intracellular redox homeostasis and cancer progression in many aggressive tumors²⁹. Therefore, whether MP3 could inhibit the activity of TrxR and thereby disturb the redox balance to induce higher ROS accumulation after being released from

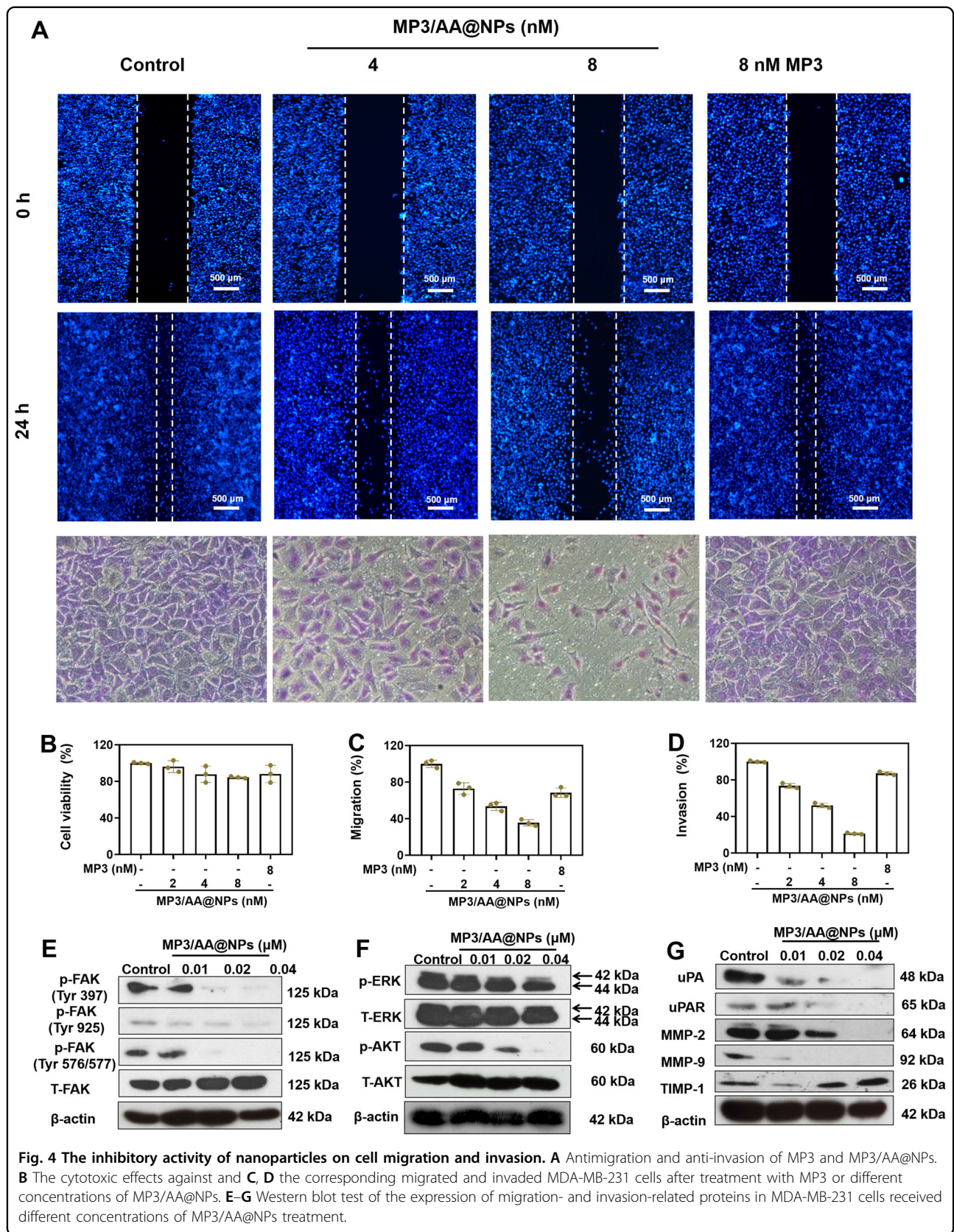


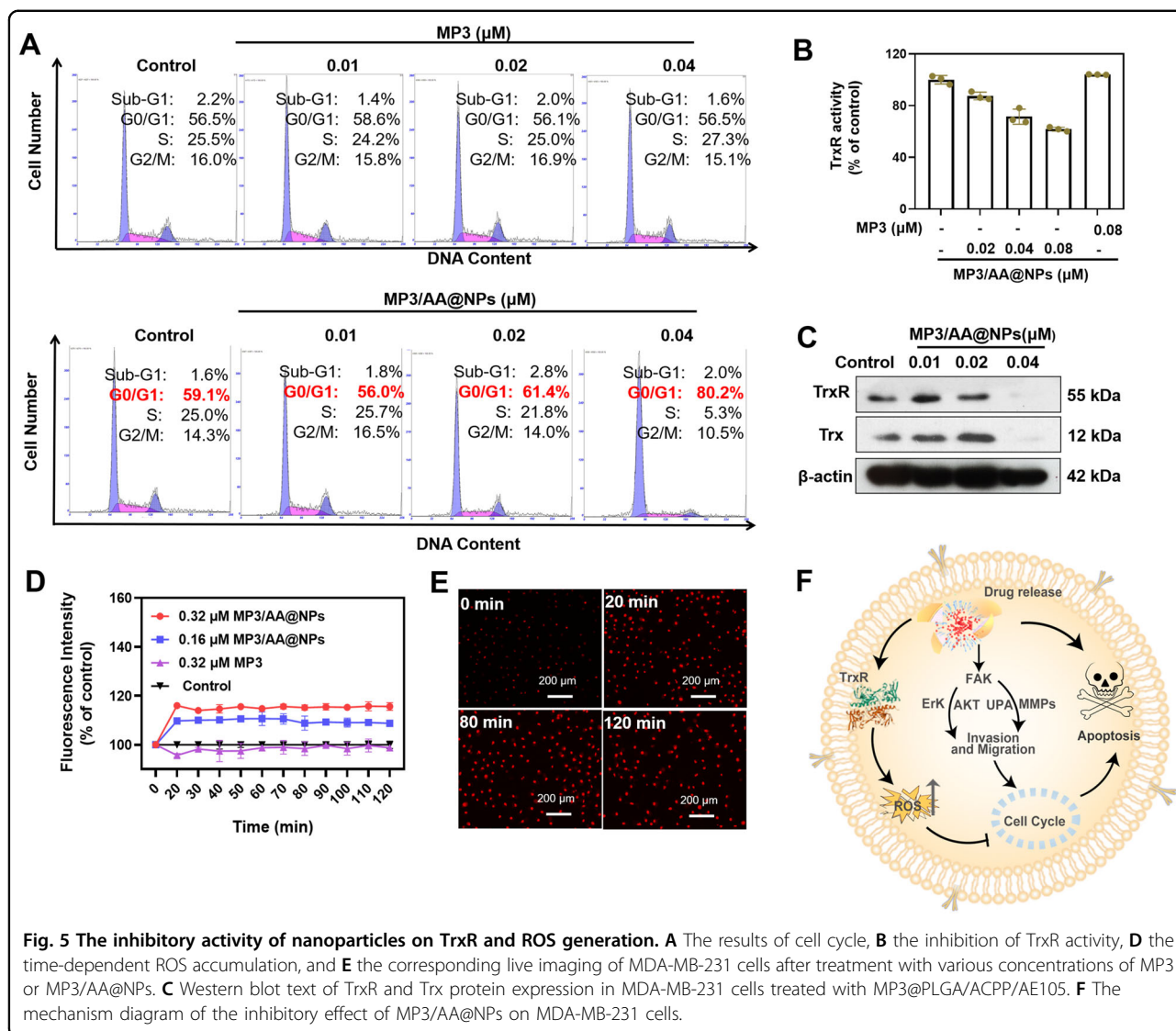
MP3/AA@NPs was tested. Figure 5D displays the mechanism diagram of the inhibitory effect of MP3/AA@NPs on MDA-MB-231 tumor cells. Notably, MP3/AA@NPs exhibited favorable inhibitory effects on TrxR activity than MP3 (Fig. 5B). Moreover, both TrxR and Trx were extremely downregulated after incubation with MP3/AA@NPs (Fig. 5C). The inhibition of TrxR might disrupt the redox homeostasis of cancer cells. Therefore, the generated ROS in cells was subsequently monitored by using dihydroethidium as a sensor after the treatment with MP3/AA@NPs or MP3. As demonstrated in Fig. 5D, MP3/AA@NPs (at 0.16 μ M and 0.32 μ M) treatment stimulated the production of intracellular ROS during 0 to 120 min. On the contrary, MP3 (at 0.32 μ M) did not trigger the overproduction of ROS. The fluorescence intensity in Fig. 5E further verified the activation of ROS generation by MP3/AA@NPs. The inhibition of cancer cell growth caused by anticancer agents could be ascribed to the effect on cell cycle distribution. Accumulating evidence showed that excess intracellular ROS could cause cell cycle arrest through multiple signaling pathways³⁰. As shown in Fig. 5A, the proportion of G0/G1-phase cells increased from

59.7% to 82.2% after treatment with different doses of MP3/AA@NPs, while no obviously G0/G1-phase arrest was observed in the MP3-treated group. Collectively, this study demonstrated that MP3/AA@NPs could induce the aggravation of ROS generation via the activity inhibition of TrxR, which promoted G0/G1 cell cycle arrest and inhibited MDA-MB-231 cell growth. This tumor microenvironment-responsive MP3/AA@NPs, as an extremely targeted nanotherapeutics, could be further used for the therapy of tumors in vivo.

In vivo therapeutic effects of MP3/AA@NPs

As the desired in vitro therapeutic efficacy of MP3/AA@NPs, the in vivo antitumor efficacy of MP3/AA@NPs was further validated using a nude mice model with xenografted MDA-MB-231 cells. MP3 and MP3/AA@NPs were injected through the tail vein every second day, and the same dose of saline was used as a control group. The changes in the tumor volumes and the body weights of mice were recorded to evaluate the effect of the treatments. Comparing the results of different groups in Fig. 6A clearly showed that





the tumor volumes on the 21th day were 2662% ± 107% (control group), 1766% ± 239% (0.5 mg/kg MP3 group), 1221% ± 170% (0.25 mg/kg NPs group), and 498% ± 124% (0.50 mg/kg NPs group), which were significantly suppressed in the groups receiving chemotherapy. Importantly, low doses (0.25 mg/kg) of NPs exhibited a superior outcome than the free MP3 (0.5 mg/kg). A significant reduction of tumor weights could also be observed in the groups of nanoparticles treatments (Fig. 6B), which further supported the enhanced antitumor effects of NPs. Moreover, the body weights of the mice in the MP3/AA@NPs group decreased slightly throughout the observation (Fig. 6C), suggesting the less systemic toxicity of MP3/AA@NPs during the therapy. Similarly, MP3/AA@NPs treatment for 21 days did not cause any obvious damage to the major organs as demonstrated by H&E staining (Fig. 6D), indicating excellent biocompatibility. In addition, MP3/AA@NPs significantly mitigated the

damages caused by tumor formation through hematological analysis (Supplementary Fig. S4). These results further confirmed the good biological safety and application potential of MP3/AA@NPs as an anticancer candidate.

As magnetic resonance imaging (MRI) could provide morphological details, high spatial resolution, and multi-functional information on lesions, making it a powerful diagnostic tool. MRI was employed to image MP3/AA@NPs in vivo by making full use of its physical properties. As shown in Fig. 6E, after 21 days of treatment, the strongly enhanced Standard ADC and Slow ADC signal at the tumor sites could be observed in MP3/AA@NPs, while significant decrease in Fast ADC signal was observed, suggesting the predominant ability of MP3/AA@NPs in enhancing necrosis and reducing blood flow of tumor tissues. This conclusion was further confirmed by quantification analysis on the relative signal intensity

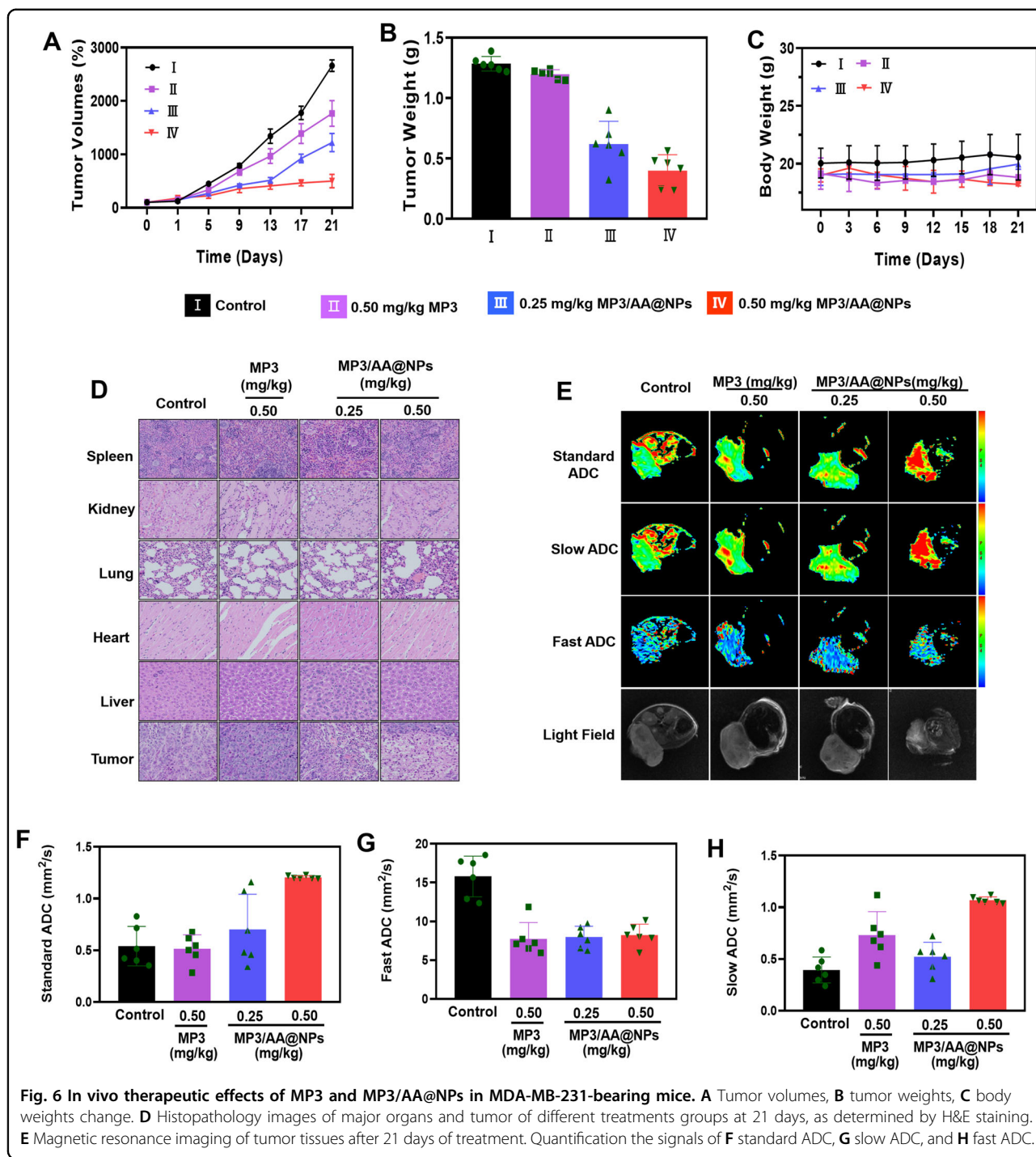
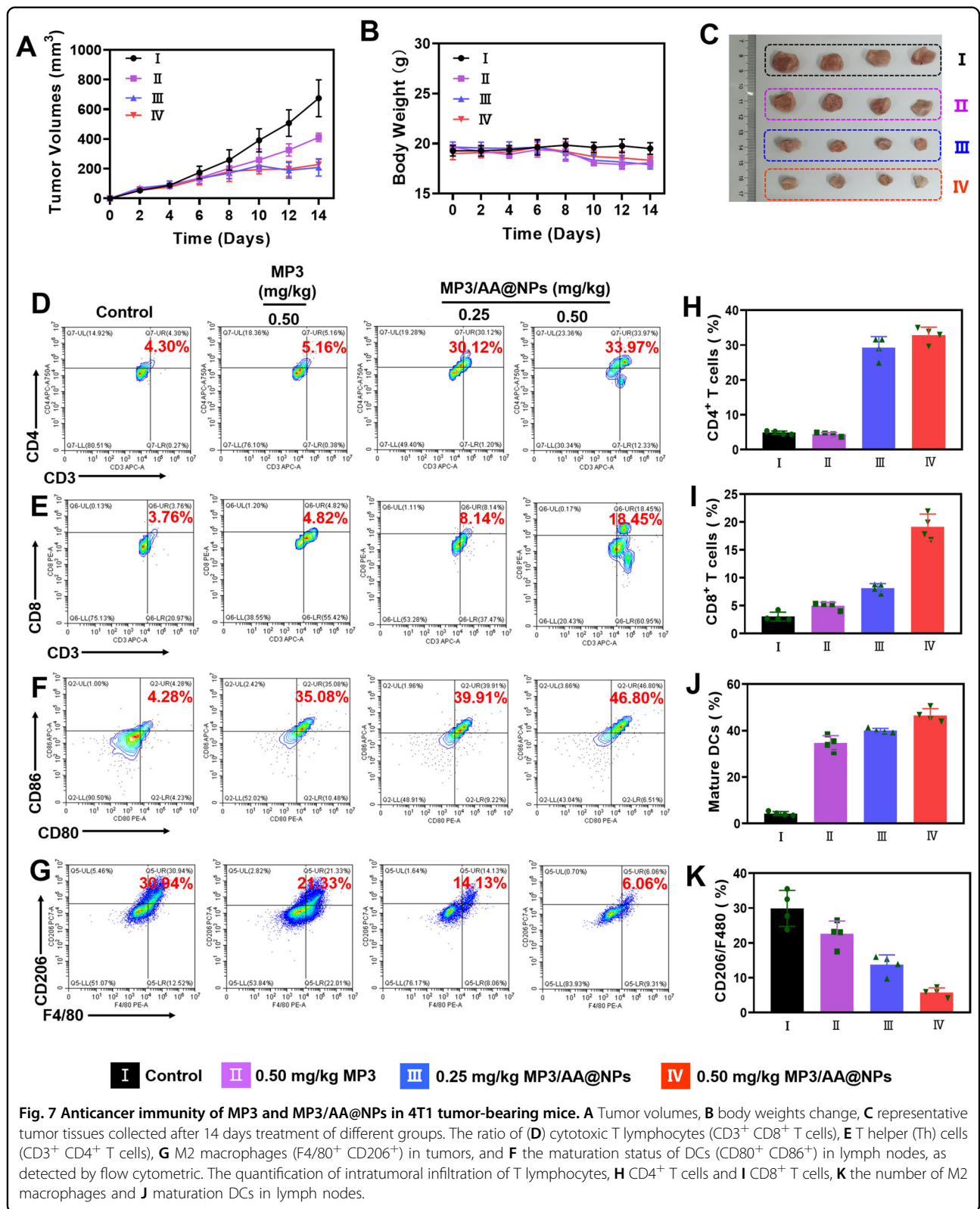


(Fig. 6F–H). All the above results further indicated the high treatment effect of MP3/AA@NPs in vivo.

MP3/AA@NPs induced antitumor immune response

Cancer immunotherapy has attracted unprecedented attention due to its promising advantage in treating primary cancer as well as inhibiting tumor metastasis and recurrence by harnessing the innate immune system^{31,32}. Tumor

ablation therapy, including traditional treatment options such as chemotherapy, could effectively initiate potent tumor-specific immune responses^{33,34}. Encouraged by the highly therapeutic efficacy of MP3/AA@NPs on the MDA-MB-231-bearing mouse model, a 4T1 tumor-bearing mouse model was established in this study to explore whether MP3/AA@NPs could trigger further immunological responses. After treatment with MP3 or MP3/AA@NPs for 14 days, as



expected, similar tumor volume delay (Fig. 7A, C), as well as low cytotoxic adverse effects, were observed (Fig. 7B). Then, the immunity-associated cells in the primary tumors and lymph nodes were isolated and detected to evaluate their immunotherapeutic effects. CD3⁺ and CD8⁺ T cells are two primarily cytotoxic T lymphocytes, with the characteristic of efficient killing tumor cells by releasing cytokines³⁵, CD4⁺ T cells, a kind of T helper (Th) cells, which could activate and regulate adaptive immune function³⁶. As can be seen from Fig. 7E, the relative proportion of CD3⁺ CD8⁺ T cells in tumor tissues were 3.76% ± 0.96% (control group), 4.82% ± 0.77% (0.5 mg/kg MP3 group), 8.14% ± 0.49% (0.25 mg/kg NPs group), and 18.45% ± 2.38% (0.50 mg/kg NP group), which was enhanced after chemotherapy, what's more, MP3/AA@NPs obtained stronger activation effects than the free MP3. Consistent with the CD3⁺ CD8⁺ T cells activation, the relative proportion of CD3⁺ CD4⁺ T cells in tumor tissues were 4.30% ± 0.61% (control group), 5.16% ± 0.77% (0.5 mg/kg MP3 group), 30.12% ± 2.58% (0.25 mg/kg NPs group), and 33.97% ± 1.57% (0.50 mg/kg NPs group). Especially, low doses (0.25 mg/kg) of MP3/AA@NPs showed better Th cell proliferation regression effects than MP3 alone (0.5 mg/kg) (Fig. 7D). These results strongly suggested that MP3/AA@NPs exerted markedly antitumor immune response via activating T cells. DCs could activate antigen-specific T cells to induce immune responses³⁷. The varying degrees of CD11c⁺ CD80⁺ CD86⁺ cells analyzed by flow cytometry were used to reflect the maturation status of DCs in lymph nodes. The maturation of DCs was elevated to 35.08% ± 3.24% in the MP3 group, while the proportion of DCs at low doses (0.25 mg/kg) and high doses (0.50 mg/kg) of MP3/AA@NPs groups were 39.91% ± 1.47% and 46.80% ± 3.68% (Fig. 7F), respectively, proving the DC maturation-boosting effects of the dual-targeted nanoparticles. TAMs can improve antitumor immunity by remodeling the tumor-related immune micro-environment³⁸. Many studies showed that the inhibition of M2 macrophages helped to kill tumors by activating the antitumor immune response³⁹. The tumor tissues were collected, and the flow cytometry analysis was carried out to further determine the effect of MP3/AA@NPs on M2 macrophages. As shown in Fig. 7G, there was a clear reduction of the proportion of M2 macrophages (CD11b⁺F4/80⁺CD206⁺) after therapy. Importantly, the ratio of M2 macrophages dropped from 30.94% ± 2.99% (control group) to 21.33% ± 3.21% (0.5 mg/kg MP3 group), 14.13% ± 2.24% (0.25 mg/kg NPs group), and 6.06% ± 1.55% (0.50 mg/kg NPs group), implying the proliferation-inhibitory effect of MP3/AA@NPs on M2 macrophages. The quantitative analysis of these immune-related cells was consistent with the aforementioned results (Fig. 7H–K). Collectively, the above results demonstrated that the in vivo therapeutic effects of MP3/AA@NPs may rely on its potent immune activation effects by modulation the activation of T cells and promoting

the maturation of DCs as well as inhibition of M2 macrophages.

Conclusions

In summary, three dual-target (DT) nanotherapeutics with universalities for encapsulating metal complexes were successfully prepared. MP3/AA@NPs with uPAR targeting and tumor microenvironment-responsive ability were selected in this study. The ACPP and AE105 peptide modifications helped to enhance the cellular uptake of drugs and improve discrimination between cancer cells and normal cells. The nanotherapeutics induced the aggravation of ROS generation by inhibiting the activity of TrxR and modulated those proteins which were related to metastasis by inhibiting FAK-mediated activation of ERK and AKT. This nanotherapeutics could also significantly improve the therapeutic benefits in vivo. Importantly, MP3/AA@NPs treatment stimulated immunotherapeutic response, which was indicated by the activation of tumor-infiltrated cytotoxic T cells, and improved the maturation of dendritic cells (DCs), and the proliferation-inhibitory effect of tumor-associated M2 macrophages. Taken together, the results suggested that this dual-targeted nanotherapeutics offered new opportunities for boosting the synergistic treatment of breast cancer with chemotherapy and immunotherapy.

Acknowledgements

This work was supported by the National Natural Science Foundation of China (32171296, 82174396, 82004385), the Natural Science Foundation of Guangdong Province of China (Nos. 2022A1515010494 and 2021A1515011455), the Science and Technology Program of Guangzhou (No. 202102010012), Innovation Team Project in Guangdong Colleges and Universities (2021KCXTD020), the Health and Medical Research Fund Project (06173996) the Specific Research Fund for TCM Science and Technology of Guangdong Provincial Hospital of Chinese Medicine (YN2018QJ05, YN2019MJ08).

Author details

¹Guangdong Provincial Key Laboratory of Tumor Interventional Diagnosis and Treatment, Zhuhai Interventional Medical Center, Zhuhai People's Hospital (Zhuhai Hospital Affiliated with Jinan University), Jinan University, 519000 Zhuhai, P.R. China. ²Orthopedics Department, Guangdong Provincial Hospital of Traditional Chinese Medicine, The Second Affiliated Hospital of Guangzhou University of Chinese Medicine, No. 111 Dade Road, 510120 Guangzhou, China. ³Department of Chemistry, Jinan University, 510632 Guangzhou, China. ⁴Research Institute for Future Food, Department of Food Science and Nutrition, The Hong Kong Polytechnic University, Hong Kong, China

Author contributions

J.L., W.L., and Y.L. conceived the study and designed the experiment. J.L., W.L., and Y.L. performed all the experiments. M.Z., H.L., Y.C., and Y.L. participated in conducting the research. J.L., W.L., Y.L., Y.P., and K.W. analyzed the experimental results. J.L., W.L., and Y.L. drafted the manuscript and compiled all the Figures. Y.P., B.C., and T.C. supervised the study, checked and revised the manuscript.

Conflict of interest

The authors declare no competing interests.

Publisher's note

Springer Nature remains neutral with regard to jurisdictional claims in published maps and institutional affiliations.

Supplementary information The online version contains supplementary material available at <https://doi.org/10.1038/s41427-023-00473-0>.

Received: 16 November 2022 Revised: 1 March 2023 Accepted: 13 March 2023

Published online: 28 April 2023

References

- Huang, Y. et al. Bioinspired tumor-homing nanosystem for precise cancer therapy via reprogramming of tumor-associated macrophages. *NPG Asia Mater.* **10**, 1002–1015 (2018).
- Han, J. et al. Cancer stem cell-targeted bio-imaging and chemotherapeutic perspective. *Chem. Soc. Rev.* **49**, 7856–7878 (2020).
- Liu, J., Lai, H., Xiong, Z., Chen, B. & Chen, T. Functionalization and cancer-targeting design of ruthenium complexes for precise cancer therapy. *Chem. Commun.* **55**, 9904–9914 (2019).
- Qu, X., Qiu, P., Zhu, Y., Yang, M. & Mao, C. Guiding nanomaterials to tumors for breast cancer precision medicine: from tumor-targeting small-molecule discovery to targeted nanodrug delivery. *NPG Asia Mater.* **9**, e452–e452 (2017).
- Song, Z. et al. Decorated ultrathin bismuth selenide nanosheets as targeted theranostic agents for in vivo imaging guided cancer radiation therapy. *NPG Asia Mater.* **9**, e439–e439 (2017).
- Lin, W. et al. Pre-clinical MRI-guided intravesical instillation theranosis of bladder cancer by tumor-selective oxygen nanogenerator. *Nano Today* **38**, 101124 (2021).
- Chen, M., Huang, X., Lai, J., Ma, L. & Chen, T. Substituent-regulated highly X-ray sensitive Os (VI) nitrido complex for low-toxicity radiotherapy. *Chin. Chem. Lett.* **32**, 158–161 (2021).
- Chen, M. et al. Selenium atom-polarization effect determines TrxR-specific recognition of metallodrugs. *J. Am. Chem. Soc.* **144**, 20825–20833 (2022).
- Bruno, P. M. et al. A subset of platinum-containing chemotherapeutic agents kills cells by inducing ribosome biogenesis stress. *Nat. Med.* **23**, 461–471 (2017).
- Lai, H. et al. Selenium-containing ruthenium complex synergizes with natural killer cells to enhance immunotherapy against prostate cancer via activating TRAIL/FasL signaling. *Biomaterials* **219**, 119377 (2019).
- He, L. et al. A cancer-targeted nanosystem for delivery of gold (III) complexes: enhanced selectivity and apoptosis-inducing efficacy of a gold (III) porphyrin complex. *Angew. Chem. Int. Ed.* **126**, 12740–12744 (2014).
- Gao, S. et al. Selenium-containing nanoparticles combine the NK cells mediated immunotherapy with radiotherapy and chemotherapy. *Adv. Mater.* **32**, 1907568 (2020).
- Kroon, P. et al. Radiotherapy and cisplatin increase immunotherapy efficacy by enabling local and systemic intratumoral T-cell activity chemo-radio-immunotherapy in PD-1-resistant cancer. *Cancer Immunol. Res.* **7**, 670–682 (2019).
- Chen, Q., He, L., Li, X., Xu, L. & Chen, T. Ruthenium complexes boost NK cell immunotherapy via sensitizing triple-negative breast cancer and shaping immuno-microenvironment. *Biomaterials* **281**, 121371 (2022).
- Lok, C. N., Zou, T., Zhang, J. J., Lin, I. W. S. & Che, C. M. Controlled-release systems for metal-based nanomedicine: encapsulated/self-assembled nanoparticles of anticancer gold (III)/platinum (II) complexes and antimicrobial silver nanoparticles. *Adv. Mater.* **26**, 5550–5557 (2014).
- Kamaly, N., Yameen, B., Wu, J. & Farokhzad, O. C. Degradable controlled-release polymers and polymeric nanoparticles: mechanisms of controlling drug release. *Chem. Rev.* **116**, 2602–2663 (2016).
- Chen, W. et al. Macrophage-targeted nanomedicine for the diagnosis and treatment of atherosclerosis. *Nat. Rev. Cardiol.* **19**, 228–249 (2022).
- Jin, E. et al. Acid-active cell-penetrating peptides for in vivo tumor-targeted drug delivery. *J. Am. Chem. Soc.* **135**, 933–940 (2013).
- Khanna, M. et al. Targeting multiple conformations leads to small molecule inhibitors of the uPAR uPA protein–protein interaction that block cancer cell invasion. *ACS Chem. Biol.* **6**, 1232–1243 (2011).
- Chen, T., Liu, Y., Zheng, W.-J., Liu, J. & Wong, Y.-S. Ruthenium polypyridyl complexes that induce mitochondria-mediated apoptosis in cancer cells. *Inorg. Chem.* **49**, 6366–6368 (2010).
- He, L. et al. Cancer-targeted monodisperse mesoporous silica nanoparticles as carrier of ruthenium polypyridyl complexes to enhance theranostic effects. *Adv. Funct. Mater.* **24**, 2754–2763 (2014).
- Huang, Y. et al. Selective cellular uptake and induction of apoptosis of cancer-targeted selenium nanoparticles. *Biomaterials* **34**, 7106–7116 (2013).
- Li, J. et al. Synergistic inhibition of migration and invasion of breast cancer cells by dual docetaxel/quercetin-loaded nanoparticles via Akt/MMP-9 pathway. *Int. J. Pharm.* **523**, 300–309 (2017).
- Zou, H. et al. Making aggregation-induced emission luminogen more valuable by gold: enhancing anticancer efficacy by suppressing thioredoxin reductase activity. *ACS Nano* **15**, 9176–9185 (2021).
- Mei, C., Wang, N., Zhu, X., Wong, K. H. & Chen, T. Photothermal-controlled nanotubes with surface charge flipping ability for precise synergistic therapy of triple-negative breast cancer. *Adv. Funct. Mater.* **28**, 1805225 (2018).
- Liu, T., Lai, L., Song, Z. & Chen, T. A sequentially triggered nanosystem for precise drug delivery and simultaneous inhibition of cancer growth, migration, and invasion. *Adv. Funct. Mater.* **26**, 7775–7790 (2016).
- Zhang, J. & Hochwald, S. N. The role of FAK in tumor metabolism and therapy. *Pharmacol. Ther.* **142**, 154–163 (2014).
- Smith, H. W. & Marshall, C. J. Regulation of cell signalling by uPAR. *Nat. Rev. Mol. Cell Biol.* **11**, 23–36 (2010).
- Li, X. et al. Selective activation of a prodrug by thioredoxin reductase providing a strategy to target cancer cells. *Angew. Chem. Int. Ed.* **130**, 6249–6253 (2018).
- Ramasamy, T. et al. Multimodal selenium nanoshell-capped Au@mSiO₂ nanoplatform for NIR-responsive chemo-photothermal therapy against metastatic breast cancer. *NPG Asia Mater.* **10**, 197–216 (2018).
- Kroemer, G. & Zitvogel, L. The breakthrough of the microbiota. *Nat. Rev. Immunol.* **18**, 87–88 (2018).
- Zhu, Y. et al. CSF1/CSF1R blockade reprograms tumor-infiltrating macrophages and improves response to T-cell checkpoint immunotherapy in pancreatic cancer models. *Cancer Res.* **74**, 5057–5069 (2014).
- Chen, Q. et al. Tumor microenvironment-triggered aggregated magnetic nanoparticles for reinforced image-guided immunogenic chemotherapy. *Adv. Sci.* **6**, 1802134 (2019).
- Sen, S. et al. Rationally designed redox-active Au (I) N-heterocyclic carbene: an immunogenic cell death inducer. *J. Am. Chem. Soc.* **142**, 20536–20541 (2020).
- Ganesan, A. P. et al. Tissue-resident memory features are linked to the magnitude of cytotoxic T cell responses in human lung cancer. *Nat. Immunol.* **18**, 940–950 (2017).
- Restifo, N. P., Dudley, M. E. & Rosenberg, S. A. Adoptive immunotherapy for cancer: harnessing the T cell response. *Nat. Rev. Immunol.* **12**, 269–281 (2012).
- Ridolfi, R. et al. Evaluation of in vivo labelled dendritic cell migration in cancer patients. *J. Transl. Med.* **2**, 1–11 (2004).
- Wei, B. et al. *Prichia coli* combined with immunogenic cell death for cancer immunotherapy. *Nano Lett.* **21**, 4231–4240 (2021).
- Funes, S. C., Rios, M., Escobar-Vera, J. & Kalergis, A. M. Implications of macrophage polarization in autoimmunity. *Immunology* **154**, 186–195 (2018).